Electric quadrupole moments of $17/2^-$ and $13/2^-$ subsequent isomers in ^{209}Po

G. Nicolescu, E. A. Ivanov, and D. Plostinaru
National Institute for Physics and Nuclear Engineering, P.O. Box MG-6, Bucharest, Romania
(Received 23 October 2008; published 21 April 2009)

The electric quadrupole interaction of ^{209}Po high spin isomers in a Bi single crystal has been investigated by the time-differential perturbed angular distribution (TDPAD) technique. A two-level analysis procedure for the $17/2^-$and $13/2^-$ subsequent isomers was employed. The spectroscopic electric quadrupole moments were measured as $|Q(17/2^-)| = 65.9(7)e$ fm^2 and $|Q(13/2^-)| = 12.6(5)e$ fm^2. The experimental values of equilibrium deformations were extracted.

DOI: 10.1103/PhysRevC.79.044314 PACS number(s): 21.10.Ky, 27.90.+b

I. INTRODUCTION

The polonium isotopes, with two valence protons beyond the closed $Z = 82$ core, provide an excellent laboratory in which to study the transition between single-particle and collective behavior in a nuclear system. In the polonium systematic, the first important change in structure occurs between the semimagic ^{210}Po and ^{208}Po. In the polonium isotopes, the two protons beyond the closed $Z = 82$ shell likely occupy the $1h_{9/2}$ orbital. One may assume that the $(1h_{9/2})^2$ configuration dominates the proton contribution. The polonium isotopes near the doubly magic ^{208}Pb exhibit nuclear properties dominated by the shell structure. The structure and energy spacings in ^{210}Po can be described by two $h_{9/2}$ protons in spherical shell models. Po is a textbook example of two protons in the $(1h_{9/2})^2$ orbital with a residual surface-delta interaction (SDI) [1]. Younes *et al.* [2] have also succeeded in reproducing the level structure of the neutron-deficient Po nuclei quite well in the particle-core model (PCM) calculations based on the assumption of two protons outside the $Z = 82$ shell closure coupled to a vibrating core. Oros *et al.* [3] conclude that the PCM model can predict quite well the experimentally observed level properties of Po isotopes with $A = 200$–210. Study of odd-mass Po nuclei provides an alternative tool for the examination of shapes of Po isotopes. For $A > 200$ the neutrons are predominantly in low-spin $2f_{5/2}, 3p_{3/2}, 3p_{1/2}$, orbitals. However for $A < 200$ the $1i_{13/2}$ orbital increasingly becomes the dominant contribution to the neutron wave function. Fotiades *et al.* [4] have studied odd-mass Po $A < 200$ nuclei and come to the conclusion that in these nuclei the odd $i_{13/2}$ neutron is weakly coupled to a vibrating core. The measurement of electric quadrupole moments is important for the information on equilibrium deformations and hence the nuclear structure of isomeric states in Po nuclei. In view of this, the electric quadrupole moments of the ^{209}Po$(17/2^-)$ and ^{209}Po$(13/2^-)$ polonium isomers have been measured and the experimental values of equilibrium deformations were extracted. The two levels analysis procedure has an unique feature: direct extraction of the electric quadrupole moments relative sign of the two subsequent isomers.

II. EXPERIMENT

The experimental technique was the time-differential perturbed angular distribution (TDPAD) for the quadrupole interaction (QI) in the presence of an electric field gradient (EFG) in Bi single crystal hexagonal host. The experiments were performed at the U-120 cyclotron in Bucharest using a pulsed deuteron beam of 13 MeV. The $17/2^-(T_{1/2} = 90$ ns) and $13/2^-(T_{1/2} = 25$ ns) isomeric states were produced and aligned by the ^{209}Bi$(d, 2n)$ reaction. The repetition time of the pulse was 10^4 ns and the width was around 5 ns (FWHM). The relatively small energy of the incident beam was chosen to optimize the population of $17/2^-$ isomer and to reduce the population of higher isomers. A partial level scheme of ^{209}Po [5] indicating the gamma transitions used in the present experiment is presented in Fig. 1.

The energetic window was set as 782 keV + 545 keV. In order to eliminate the dependence on the specific time response function of an individual spectrometer, only one scintillation spectrometer was used and placed alternatively at angles 0° and 90° with respect to the beam axis. The scintillation crystal was a 3 in. × 3 in. NaI(Tl) with energy resolution <8.0% at 662 keV (^{137}Cs) and time resolution <2 ns at 511 keV (^{22}Na). Time spectra have been collected in a conventional fast-slow coincidence circuit and were accumulated in an on-line computer. The target was mounted on a combined cooling-heating system so that the temperature could be stabilized at 470° K ± 2° K in order to minimize the lattice damage induced by the beam bombardment. In the conditions of the present experiment the temporal window for the observation of extranuclear perturbation is greater than the precession semiperiod of the basic frequency allowing highly accurate measurements. Results on the QI frequency have been collected in two runs:

(i) The $\hat{c}$ axis of the Bi monocrystalline target at 45° to the beam direction;
(ii) The $\hat{c}$ axis of the Bi monocrystalline target at 90° to the beam direction and normal to the detection plane.

III. DATA ANALYSIS AND RESULTS

Vyvey *et al.* [6] developed a double perturbation analysis for two subsequent isomers, to extract the ratios of the quadrupole interaction frequencies to the magnetic moments based on the LEMS (level mixing spectroscopy) method. In our experiment only quadrupole moments are involved and we preferred the two-level analysis procedure proposed by

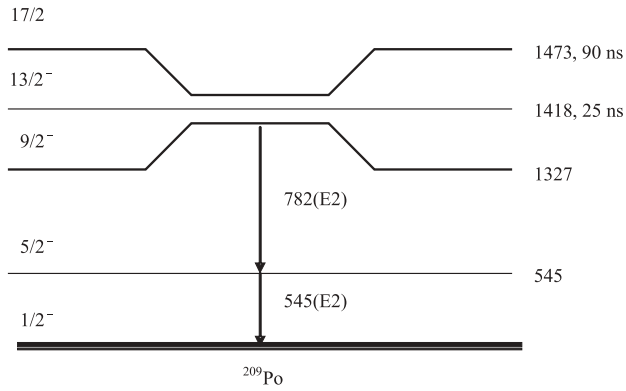

FIG. 1. Partial levels scheme of ^{209}Po indicating the gamma transitions used in the present experiment. Energies in keV and half-lives are shown.

Dafni *et al.* [7] for two subsequent isomers in a single-crystal host. Basically, the two-level perturbation function for static axial-symmetric quadrupole interactions is

$$G^{q\,q}_{k_2k_0}(I_1, I_2; t) = \frac{\frac{1}{\tau_2} - \frac{1}{\tau_1}}{e^{-\frac{t}{\tau_1}} - e^{-\frac{t}{\tau_2}}} \sum_{k_1} U_{k_1}(\gamma) F^{k_2k_0}_{k_1 q}(I_1, I_2; t). \quad (1)$$

The sum over k_1 is up to $2I_{\min}$. The quantization axis is the interaction symmetry axis, actually the $\hat{c}$ axis of the single crystal. The time modulation is introduced by

$$F^{k_2k_0}_{k_1q}(I_1, I_2; t) = \sum_{n_1,n_2} C^{k_2k_1}_{n_2q} C^{k_1k_0}_{n_1q} \frac{e^{-f_{n_1}t} - e^{-f_{n_2}t}}{f_{n_2} - f_{n_1}}. \quad (2)$$

The U_k coefficients are used for the unobserved gamma rays during the decay from the first to the second isomer. The complex frequencies are

$$f_{n\,j} = 1/\tau_j + in\omega_{0j}. \quad (3)$$

The combination coefficients are related to the usual $S^{kk'}_{nq}$ as

$$C^{kk'}_{nq} = \tfrac{1}{2}[1 + (-1)^{k+k'}\delta_{n0}]\,(-1)^{k+k'} S^{kk'}_{|n|q}. \quad (4)$$

The explicit form of the time modulation function for our experiment is

$$\begin{aligned} F^{k_2k_0}_{k_1q}(I_1, I_2; t) &= \sum_{n_1,n_2} \frac{C^{k_2k_1}_{n_2q} \cdot C^{k_1k_0}_{n_1q}}{\left(\frac{1}{\tau_1} - \frac{1}{\tau_2}\right)^2 + (n_2 \cdot \omega_{02} - n_1 \cdot \omega_{01})^2} \\ &\times \left\{ e^{-\frac{t}{\tau_1}} \left[\left(\frac{1}{\tau_2} - \frac{1}{\tau_1}\right) \cos(n_1 \cdot \omega_{01} \cdot t) \right.\right. \\ &\left. - (n_2 \cdot \omega_{02} - n_1 \cdot \omega_{01}) \sin(n_1 \cdot \omega_{01} \cdot t) \right] \\ &- e^{-\frac{t}{\tau_2}} \left[\left(\frac{1}{\tau_2} - \frac{1}{\tau_1}\right) \cos(n_2 \cdot \omega_{02} \cdot t) \right. \\ &\left.\left. - (n_2 \cdot \omega_{02} - n_1 \cdot \omega_{01}) \sin(n_2 \cdot \omega_{02} \cdot t) \right] \right\}. \quad (5) \end{aligned}$$

Obviously, the sum limits in Eq. (5) depend on the angle between the $\hat{c}$ axis and the beam direction (45° and 90° in our experiments).

The analysis of time modulation functions is shown in Figs. 2 and 3 for both angles.

For $k_1 = 1$–4 it is obvious that only the term with $k_1 = 2$ is dominant. Also, for higher k_1 the $F^{k_2k_0}_{k_1q}$ functions are strongly attenuated during the unobserved decay, as manifested by the U_k coefficients. Consequently, the sum limit for Eq. (1) is $k_1 = 4$. The two-level perturbation functions for $T_{1/2}$ (first isomer) $\to 0$ and $T_{1/2}$ (second isomer) $\to 0$ become the well known theoretical single-level pure pattern for 45° and, respectively, 90° (normal to the detection plane). This fact confirms the consistency of the two-level analysis. The two-level perturbation functions are sensitive to the relative sign of the electric quadrupole moments of the two subsequent isomers. This feature is shown in Figs. 4 and 5 for each angles used in our experiment. In a physical case the influence of the other decay branches on the angular distribution function could be important. An exhaustive analysis of this influence

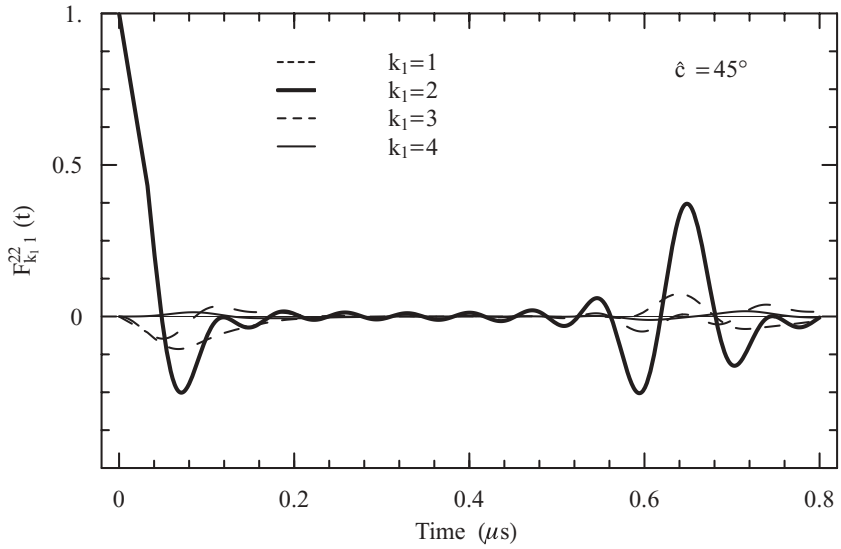

FIG. 2. Time modulation functions $F^{k_2k_0}_{k_11}$ for a hypothetical two-isomers case. Parameters: 45° between the $\hat{c}$ and the beam direction; $I_1 = 17/2^-$; $I_2 = 13/2^-$; $T_{1/2}(17/2^-) = 90$ ns; $T_{1/2}(13/2^-) = 25$ ns. The $F^{k_2k_0}_{2\,1}$ is the dominant term.

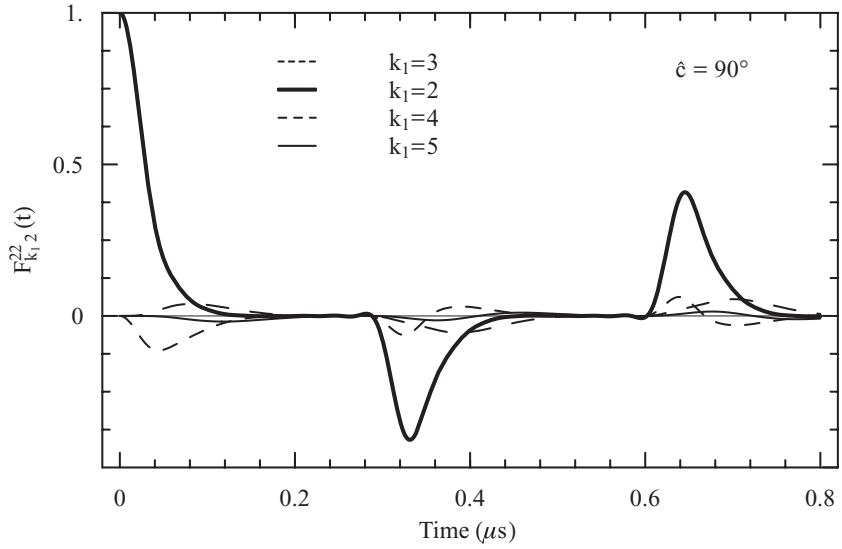

FIG. 3. Time modulation functions $F^{k_2 k_0}_{k_1 2}$ for a hypothetical two-isomers case. Parameters: 90° between the $\hat{c}$ and the beam direction (normal to the detection plane); $I_1 = 17/2^-$; $I_2 = 13/2^-$; $T_{1/2}(17/2^-) = 90$ ns; $T_{1/2}(13/2^-) = 25$ ns. The $F^{k_2 k_0}_{22}$ is the dominant term.

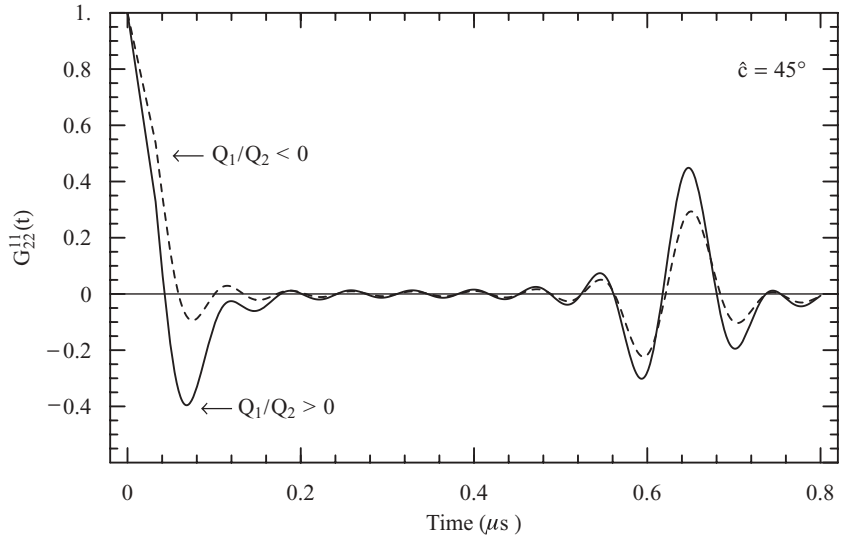

FIG. 4. Theoretical two-level perturbation functions for 45° between the $\hat{c}$ and the beam direction. Parameters: $I_1 = 17/2^-$; $I_2 = 13/2^-$; $T_{1/2}(17/2^-) = 90$ ns; $T_{1/2}(13/2^-) = 25$ ns; $Q_1/Q_2 > 0$ and $Q_1/Q_2 < 0$.

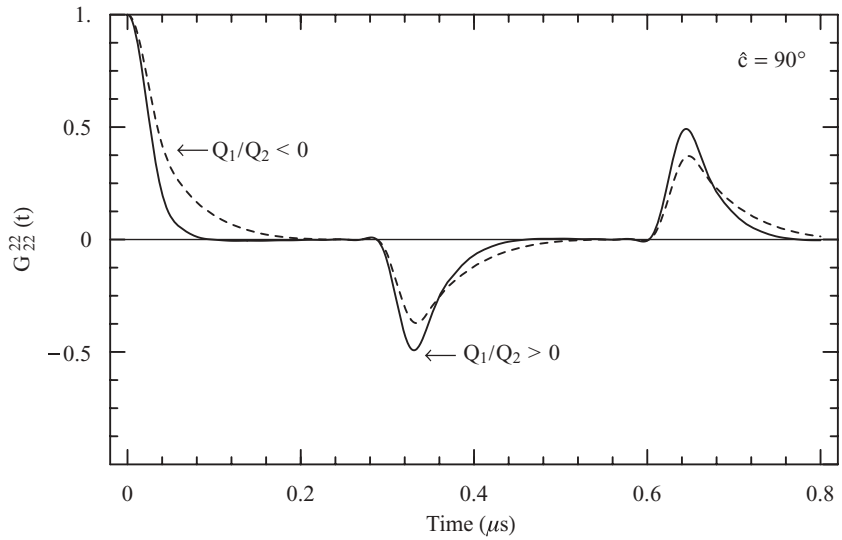

FIG. 5. Theoretical two-level perturbation functions for 90° (normal to the detection plane). Parameters: $I_1 = 17/2^-$; $I_2 = 13/2^-$; $T_{1/2}(17/2^-) = 90$ ns; $T_{1/2}(13/2^-) = 25$ ns; $Q_1/Q_2 > 0$ and $Q_1/Q_2 < 0$.

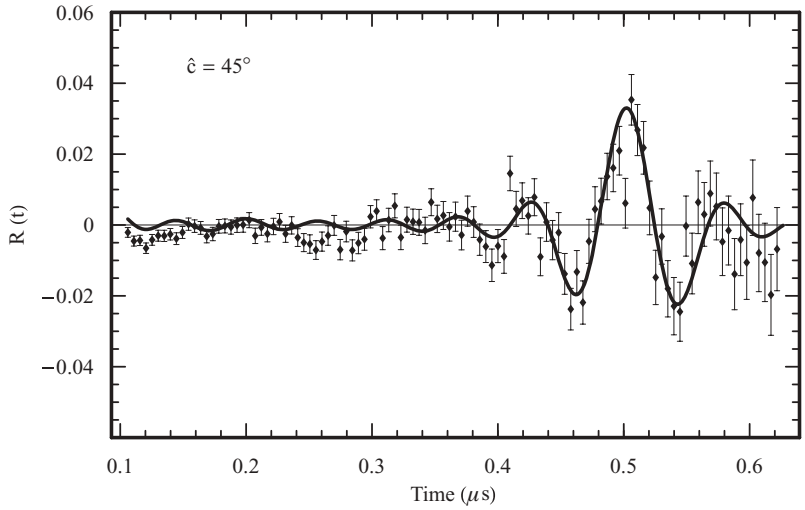

FIG. 6. Fitted curve and ratio function for 45° between the $\hat{c}$ and the beam direction.

is done in [6]. In our experiment only quadrupole moments are involved and for our geometries the most suitable ratio function form [7] is

$$R(t) \approx \frac{3}{4} A_{22} \frac{\left(\frac{(1-f)}{\tau_2}\right) e^{-\frac{t}{\tau_2}} G(I_2;t) + \left(\frac{f}{(\tau_1-\tau_2)}\right)\left(e^{-\frac{t}{\tau_1}} - e^{-\frac{t}{\tau_2}}\right) G(I_1, I_2;t)}{\left(\frac{(1-f)}{\tau_2}\right) e^{-\frac{t}{\tau_2}} + \left(\frac{f}{(\tau_1-\tau_2)}\right)\left(e^{-\frac{t}{\tau_1}} - e^{-\frac{t}{\tau_2}}\right)}, \tag{6}$$

where 1-f is the fraction of side feeding directly into the lower isomer. For each measurement a ratio function was formed:

$$R\,(t) = \frac{W\,(0^\circ, t) - W\,(90^\circ, t)}{W\,(0^\circ, t) + W\,(90^\circ, t)\,}, \tag{7}$$

where W(theta, t) are the normalized, background-subtracted time spectra.

The f fraction for Eq. (6) and the half-lives of the two isomers for checking reasons were determined from a two-lifetime fit to the time spectra (see Table I).

For half-integer spin, the quadrupole interaction frequency ω_0 is given by

$$\omega_0 = \frac{6eQV_{zz}}{4I\,(2I-1)\hbar}, \tag{8}$$

where Q is the spectroscopic quadrupole moment and $V_{zz}(= eq)$ is the principal component of the diagonalized electric field gradient (EFG) tensor. The calibration value of the electric field gradient $eq(\mathrm{Po}Bi) = 11.7 \times 10^{17}$ V/cm^2 at 478° K ±5° K [8] was considered, because in our experiment the temperature of the target was stabilized at 470° K ± 2° K. Data and fits to Eq. (6) are shown in Fig. 6 for the $\hat{c}$ axis at 45° to the beam direction and in Fig. 7 for the $\hat{c}$ axis at 90° to the beam direction and normal to the detection plane. Basically,

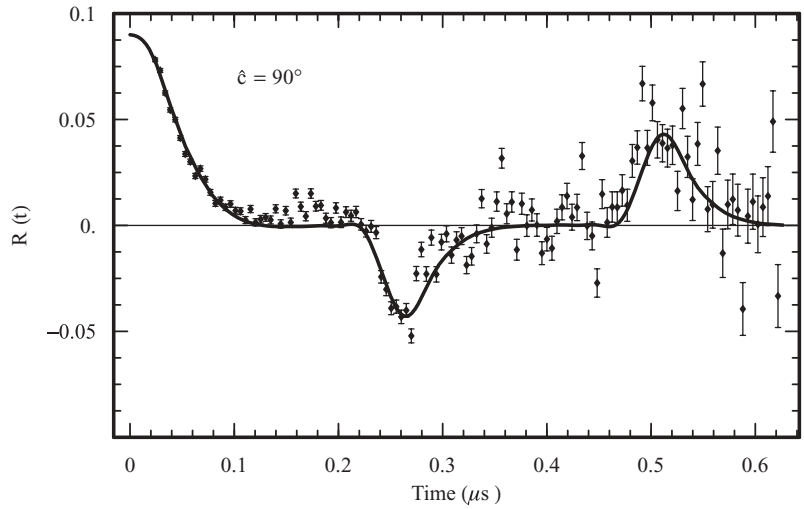

FIG. 7. Fitted curve and ratio function for 90° (normal to the detection plane).

TABLE I. Fitting results for quadrupole frequencies and half-lives of ^{209}Po($17/2^-$) and ^{209}Po($13/2^-$).

Geometry	$T_{1/2}$ (ns)		f [b]	e^2Qq/h (MHz)[a]	
	^{209}Po($17/2^-$)	^{209}Po($13/2^-$)		^{209}Po($17/2^-$)	^{209}Po($13/2^-$)
45°	89.8(5)	24.5(4)	0.58(2)	183.3(2)	35.6(5)
90°	88.7(7)	23.6(5)	0.60(2)	186.1(2)	34.8(4)

[a]Strictly stastistical errors.
[b](1-f) is the fraction of side feeding directly into the lower isomer.

we used the advantage of the present experiment which access the precession semiperiod of the basic frequency. The quadrupole interaction frequencies are presented in Table I. The evaluated spectroscopic quadrupole moments are

$$|Q(17/2^-)| = 65.9(7)e\ \mathrm{fm}^2,$$
$$|Q(13/2^-)| = 12.6(5)e\ \mathrm{fm}^2.$$

Dafni *et al.* [9] proposed for the $17/2^-$ isomer in ^{209}Po a value that is almost a factor of 1.5 smaller than the present one. The difference may have several possible causes: (a) Their experimental conditions were less clean; (b) They did not have experimentally access to the value of the second isomer ($13/2^-$) and were forced to presume the 0.2 quadrupole moments ratio as a fixed parameter for the fit; (c) They used a polycrystalline target and did not have the possibility to corroborate two runs (45° and 90°) as we did using a monocrystalline target.

The quadrupole moment is an excellent tool to study the deformation of nuclei. The spectroscopic quadrupole moment is the experimental observable, which in case of axially deformed nuclei, can be related to the intrinsic quadrupole moment, and thus to the nuclear charge deformation parameter β_2. For well deformed axially symmetric nuclei, the measured (=spectroscopic) quadrupole moment Q can be related to the intrinsic quadrupole moment Q_0 through the relation (Bohr-Mottelson):

$$Q = Q_0 \frac{3K^2 - I(I+1)}{(I+1)(2I+3)}. \tag{9}$$

This is valid in the strong coupling limit, with K the projection of the total spin I onto the symmetry-axis of the deformed nucleus. For the semimagic ^{210}Po the spherical shell models are the best aproach. As the number of neutrons decreases, the large number of valence particles makes a shell model description less meaningful and the onset of a collective structure is expected. This is attributed to an increasing quadrupole collectivity induced by interactions between the proton particles and holes in the neutron shell. Also, the deformation of the isomeric states with holes in the $N = 126$ shell is mainly determined by the core part, and very little by the valence particles.

The ^{209}Po has a sensitive position, between ^{210}Po and ^{208}Po, and we may consider that Eq. (9) starts to be a valid aproximation. In the hydrodynamical model of the nucleus the intrinsic quadrupole moment Q_0 is related to the nuclear deformation parameter β_2 as follows [10]:

$$Q_0 = \frac{3}{\sqrt{5\pi}} eZR^2\beta_2 \left\{ 1 + \pi^2 \left(\frac{a}{R}\right)^2 + \frac{2}{7}\sqrt{\frac{5}{\pi}}\beta_2 \right\}. \tag{10}$$

This expression takes into account a correction due to the surface thickness ($a = 0.54$ for the Pb region [11]) and the nuclear radius is taken as $R = 1.1A^{1/3}$ fm. The surface correction term is often not taken into account because it is very small, in particular for heavy nuclei. In our calculation, we will therefore neglect this correction. Finally the relation is

$$Q_0 = \frac{3}{\sqrt{5\pi}} eZR^2\beta_2\,(1 + 0.36\beta_2)\,. \tag{11}$$

If the deformation of the isomeric state is directly deduced from the experimental quadrupole moments Eq. (11) yields

$$|\beta_2(17/2^-)| = 0.033(3),$$
$$\left|\beta_2(13/2^-)\right| = 0.007(4).$$

We may assume from [12] that deformation of the isomeric states with holes in the $N = 126$ shell is mainly determined by the core part, and very little by the valence particles. The sign of the quadrupole moment cannot be measured in the present experiment, but from shell model considerations we assume a negative sign for both quadrupole moments. The relative quadrupole moment sign of the two subsequent isomers is evaluated as positive. This evaluation confirms experimentally that $17/2^-$ and $13/2^-$ polonium subsequent isomers have the same shape assumed as oblate. The evaluation is specific for this two-level analysis procedure.

[1] R. F. Casten, *Nuclear Structure from a Simple Perspective* (Oxford University Press, Oxford, 1990).
[2] W. Younes and J. A. Cizewski, Phys. Rev. C **55**, 1218 (1997).
[3] A. Oros *et al.*, Nucl. Phys. **A645**, 107 (1999).
[4] N. Fotiades *et al.*, Phys. Rev. C **56**, 723 (1997).
[5] R. B. Firestone and V. S. Shirley, *Table of Isotopes*, 8th ed. (Wiley, New York, 1996).
[6] K. Vyvey *et al.*, Phys. Rev. C **65**, 024320 (2002).
[7] E. Dafni *et al.*, Nucl. Phys. **A441**, 501 (1985).
[8] K. H. Maier, HMI preprint **6**, 85 (1985).
[9] E. Dafni *et al.*, Nucl. Phys. **A394**, 245 (1983).
[10] H. Sagawa *et al.*, Phys. Lett. **B202**, 15 (1988).
[11] A. Bohr and B. R. Mottelson, *Nuclear Structure* (Benjamin, New York, 1969).
[12] G. Neyens, Rep. Prog. Phys. **66**, 633 (2003).